Extending the Photoresponse of TiO_2 to the Visible Light Region: Photoelectrochemical Behavior of TiO_2 Thin Films Prepared by the Radio Frequency Magnetron Sputtering Deposition Method

Hisashi Kikuchi,[†,‡] Masaaki Kitano,[‡] Masato Takeuchi,[‡] Masaya Matsuoka,[‡] Masakazu Anpo,[*,‡] and Prashant V. Kamat[*,†]

Radiation Laboratory and Department of Chemistry and Biochemistry, University of Notre Dame, Notre Dame, Indiana 46656-0579, and Department of Applied Chemistry, Graduate School of Engineering, Osaka Prefecture University, 1-1 Gakuen-cho, Sakai, Osaka 599-8531, Japan

Received: October 3, 2005

TiO_2 thin films prepared by a radio frequency magnetron sputtering (RF-MS) deposition method were found to show an enhanced photoelectrochemical response in the visible light region. By controlling the temperature and the gaseous medium during the deposition step, it was possible to control the properties of these films. The photoelectrochemical behavior of the sputtered TiO_2 thin films was compared with that of a commercial TiO_2 sample, and the sputtered films showed higher incident photon to the charge carrier generation efficiency (IPCE of 12.6% at 350 nm) as well as power conversion efficiency (0.33% at 1.84 mW/cm^2) than the commercial TiO_2 sample. Femtosecond transient absorption spectroscopy experiments have revealed that a major fraction of photogenerated electrons and holes recombine within a few picoseconds, thus limiting photocurrent generation efficiency. The mechanistic insights obtained in the present study should aid in designing semiconductor nanostructures that will maximize the charge separation efficiency and extend the response of the large band gap semiconductor TiO_2 into visible light regions.

Introduction

Semiconductor particulate systems have been widely employed in designing photocatalytic systems and photoelectrochemical cells.[1−10] For example, nanostructured films obtained from colloidal suspensions are quite effective in generating photocurrents under band gap excitation. Large band gap semiconductors such as TiO_2 show a high degree of stability but require excitation with wavelengths shorter than 380 nm for inducing charge separation. Extending the photoresponse of large band gap semiconductors into the visible light region is, thus, important for the design of photoconversion systems that can efficiently harvest solar energy. With increased interest in a hydrogen economy, photocatalysts that can respond efficiently in visible light regions are greatly desired.[11,12]

During the past decade, many new approaches have been considered for extending the response of TiO_2 into the visible region. Intrinsic doping with transition metal ions during chemical synthesis was initially considered effective. However, chemically doped transition metal ions were observed to accelerate the rate of charge recombination and decrease the overall catalytic efficiency.[13] In contrast, the physical doping of transition metal ions such as V or Cr into TiO_2 by advanced ion-implantation techniques has been shown to enable TiO_2 photocatalysts to work under visible light irradiation.[14,15] Another promising approach involves anion doping of the TiO_2 films and nanostructures. Efforts have also been made to narrow the band gap using doping with carbon,[16] nitrogen,[17] and sulfur.[18] Such a procedure shifts the valence band to a less negative potential, thereby, decreasing the band gap. For example, by using nitrogen-doped TiO_2 ($TiO_{2-x}N_x$), Asahi et al.[19] have reported photocatalytic reactivity toward the degradation of methylene blue and gaseous acetaldehyde under visible light irradiation.

In an earlier study, we have reported on the photocatalytic aspects of TiO_2 thin films prepared by a radio frequency magnetron sputtering (RF-MS) deposition,[20,21] and their photoelectrochemical properties are now presented. We report, herein, the ability of these TiO_2 thin films toward the harvesting of visible light.

Experimental Section

Materials and Electrode Preparation. Optically transparent electrodes (OTEs) were cut from a transparent electrical conducting glass plate (TEC glass) obtained from Pilkington (Libbey Owens Ford). These electrodes were ultrasonically cleaned in acetone, ethanol, and distilled water, then finally dried at 373 K for 1 h in an oven. The substrate was kept initially at room temperature under vacuum.

Three types of TiO_2 thin films were prepared using the RF-MS method. A high-purity sintered TiO_2 (99.99%) was used as the sputtering target, and Ar and O_2 were used as the sputtering gases. The base pressure in the chamber was set at $\sim 8 \times 10^{-4}$ Pa, and the working pressure was 1.0 and 2.0 Pa. The substrate was placed parallel to the sputtering target surface with substrate−target distances of 75 and 100 mm. The TiO_2 thin films were deposited on the OTE at two different temperatures (673 and 873 K) using an RF power of 300 W. During deposition, the substrate holder was kept rotating for uniform deposition onto the substrate. The thickness of the sputtered

* To whom correspondence should be addressed. E-mail: pkamat@nd.edu; anpo@chem.osakafu-u.ac.jp.
† University of Notre Dame.
‡ Osaka Prefecture University.

10.1021/jp058262g CCC: $33.50
Published on Web 02/25/2006

TiO_2 thin films was around 1 μm. These TiO_2 thin films are referred to as OTE/(673 K-Ar)−TiO_2, OTE/(873 K-Ar)−TiO_2, and OTE/(873 K-Ar + O_2)−TiO_2.

We also prepared a standard Degussa P-25 thin film photocatalyst on the OTE as a reference. A suspension of TiO_2 (Degussa P-25) was prepared by suspending 1.6 g/L of TiO_2 in water by sonication for 15 min. A P-25 suspension of 0.5 mL was applied on a conducting surface of 8 × 40 mm^2 for the OTE substrate and was then air-dried. The P-25 thin film cast onto the OTE was sintered at 673 K for 1 h in a furnace. The thickness of the P-25 thin films was estimated at ∼1 μm, as determined from gravimetric analysis. We named this sample OTE/P-25.

Atomic force microscopy (AFM) was performed using a digital nanoscope (Nanoscope IIIa) in the tapping mode. An etched silicon tip was used as a probe for the imaging of the TiO_2 thin film surfaces. Optical absorbance measurements were carried out with a Cary 50 spectrometer.

Photoelectrochemical Measurements. A standard two-arm cell consisting of a working electrode (viz., OTE/(673 K-Ar)−TiO_2, OTE/(873 K-Ar)−TiO_2, OTE/(873 K-Ar + O_2)−TiO_2, and OTE/P-25) and a counter (Pt gauze) electrode was employed for photoelectrochemical measurements. A Princeton Applied Research (PAR) Model 173 potentiostat and Model 175 universal programmer were used for recording photoelectrochemical measurements using a Keithley Model 617 programmable electrometer. A 0.05 M NaOH solution in water was used as the electrolyte, and N_2 gas was bubbled through the solution for 20 min. Irradiation of the electrodes was carried out from the substrate side. A collimated light beam from a 150 W xenon lamp was used for excitation of the electrode. A 10 cm path length $CuSO_4$ solution filter placed in the optical path filtered out light below 300 nm. A Bausch and Lomb high-intensity grating monochromator was introduced in the path of the excitation to carry out wavelength-dependent photocurrent measurements.

Femtosecond Transient Absorption Spectroscopy. The time-resolved transient absorption spectra were recorded with a femtosecond transient absorption spectrometer, the major component of which is the Clark MXR-2010 Ti:sapphire laser system. This turn-key ON laser system is capable of delivering 775 nm laser pulses of 1 mJ/pulse (pulse width 130 fs) at a rate of 1 kHz. A fraction of the primary output (∼5%) was utilized to generate a white probe pulse while the rest was utilized to generate a second harmonic pulse (387 nm, ∼0.2 mJ) which was used as an excitation pulse. Detection of the transient absorption was performed using a time-resolved spectrometer (Ultrafast Systems). The time-resolved spectra were recorded using an optical delay rail with an accumulation time interval of 5 s for each spectrum.

Results and Discussion

Characterization of the TiO_2 Thin Films. Figure 1 shows the diffuse reflectance absorption spectra of various TiO_2 thin films deposited on the OTE. The TiO_2 films show strong absorption in the UV region as expected from the large band gap of TiO_2 (3.2 eV). However, three of the four electrodes show extended absorption in the visible light region (λ > 380 nm). The absorption of OTE/(673 K-Ar)−TiO_2, OTE/(873 K-Ar)−TiO_2, and OTE/(873 K-Ar + O_2)−TiO_2 is observed to extend beyond 400 nm (spectra b, c, and d). Details on the visible response of such magnetron sputtered films have been discussed in an earlier study.[20,21] In the previous work, we have concluded that the sputtered films exhibit unique declined O/Ti

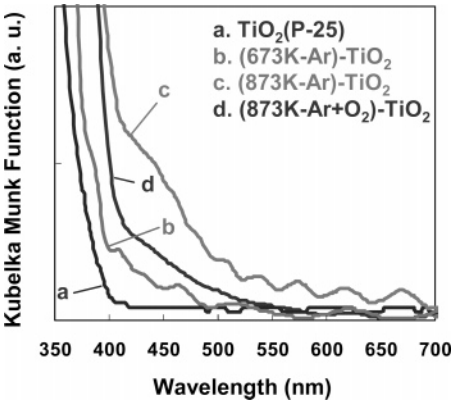

Figure 1. Diffuse reflectance absorption spectra of different TiO_2 films deposited on an optically transparent electrode (OTE).

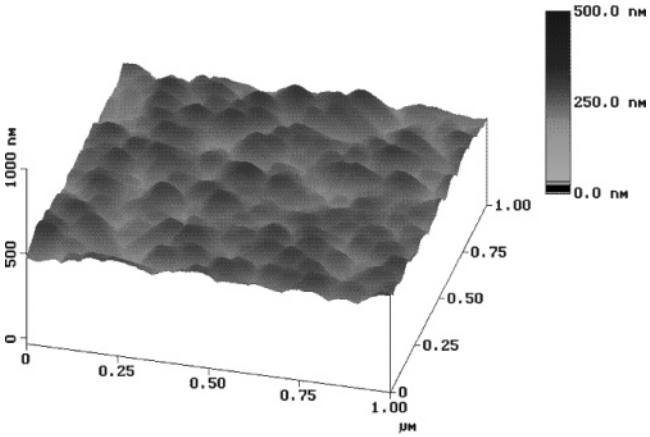

Figure 2. Atomic force microscopic image of the OTE/(673 K-Ar)−TiO_2 film.

composition from the surface to deep inside the bulk and that such a unique anisotropic structure plays an important role in the modification of the electronic properties to enable the absorption of visible light. The long wavelength absorption seen with the sputtered samples can also arise from the scattering effects. By recording the photocurrent response at different wavelengths, we should be able to resolve whether the visible response of the sputtered films can induce charge separation. Such an action spectrum analysis is used to distinguish the active crystalline phases in TiO_2 systems.[22]

The morphology of the sputtered TiO_2 thin films was characterized using AFM, and these images revealed a nanostructured morphology. The primary particles to construct the thin films of (873 K-Ar)−TiO_2 (100−200 nm) are larger than those of the other sputtered TiO_2 thin films ((673 K-Ar)−TiO_2 (35−90 nm) and (873 K-Ar + O_2)−TiO_2 (30−50 nm)). A representative AFM image of (673 K-Ar)−TiO_2 is shown in Figure 2. The other two images are presented in the Supporting Information (Figure S1). These grain size variations show how the sputtering conditions control the particle size, that is, the mere presence of oxygen during the sputtering process produces smaller size crystallites.

Photoelectrochemical Properties of the TiO_2 Thin Films. Nanostructured TiO_2 films are photoactive as they undergo charge separation when subjected to the following band gap excitation (eq 1)

$$TiO_2 + h\nu \rightarrow TiO_2\ (e_{CB} + h_{VB}) \qquad (1)$$

where e_{CB} and h_{VB} represent the conduction band electrons and valence band holes. The photogenerated electrons can be readily

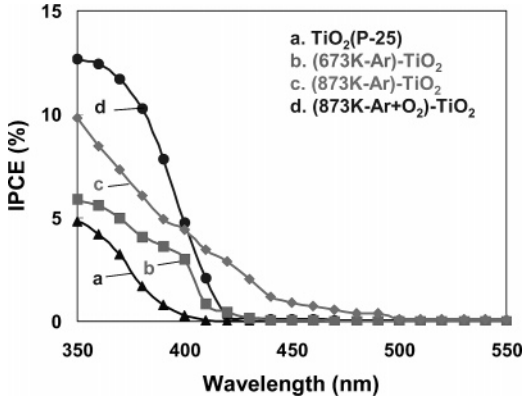

Figure 3. Photocurrent action spectra recorded for different TiO_2 films. (The counter electrode was a Pt wire gauze, and the electrolyte was a N_2-purged 0.05 M NaOH aqueous solution.)

collected at a conducting surface in a photoelectrochemical cell.[23,24] Photoelectrochemical measurements were performed using a standard two-electrode system consisting of a working electrode (nanostructured TiO_2 electrode) and Pt wire gauze counter electrode in an N_2-purged 0.05 M NaOH aqueous solution. The short circuit photocurrents of the thin films at different excitation wavelengths were recorded to assess the photoresponse. The incident photon to the charge carrier generation efficiency (IPCE), defined as the number of electrons collected per incident photon, was determined by measuring the short circuit photocurrent (I_{sc}) of the OTE/TiO_2 electrodes at each excitation wavelength and by using the following equation

$$\text{IPCE (\%)} = \{[1240 \times I_{sc}\,(\text{A/cm}^2)]/[\lambda\,(\text{nm}) \times I_{inc}\,(\text{W/cm}^2)]\} \times 100 \quad (2)$$

where I_{inc} is the incident light intensity (W/cm^2) and λ is the excitation wavelength (nm).[24] The constant "1240" is the conversion rate of photon energy to electrochemical current used to determine the IPCE value.[24] The photocurrent action spectra of the different TiO_2 films are shown in Figure 3.

The sputtered TiO_2 thin films were clearly seen to exhibit a response in the visible light region. The onset wavelength for photocurrent generation varied from 420 to 500 nm for the sputtered films. This is in contrast to the OTE/P-25 which had an onset wavelength of 380 nm. The photocurrent response of OTE/(873 K-Ar)−TiO_2 confirms its ability to harvest photons up to 500 nm and shows the highest IPCE in the visible light region (2.9% at $\lambda = 420$ nm). This is, indeed, a remarkable improvement over the pristine TiO_2 film (anatase) which can harvest only UV photons. The sputtered TiO_2 thin films also showed higher IPCE than the reference OTE/P-25. The OTE/(873 K-Ar + O_2)−TiO_2 electrode exhibits a higher IPCE in the UV region (12.6% at $\lambda = 350$ nm) than the other electrodes. The observed photocurrent response in the visible light region is further evidence that the absorption seen in the visible region (Figure 1) contributes to the charge separation in these magnetron sputtered TiO_2 films. Furthermore, these photogenerated electrons are collected at the OTE to generate photocurrents.

Photocurrent Response and Power Characteristics of TiO_2 Thin Film Electrodes. Figure 4 shows the photocurrent−time profiles of TiO_2 thin films under UV and visible light irradiation. All of the sputtered TiO_2 electrodes exhibited a prompt photocurrent response when subjected to UV−vis light irradiation. The films sputtered in the presence of Ar and O_2, namely,

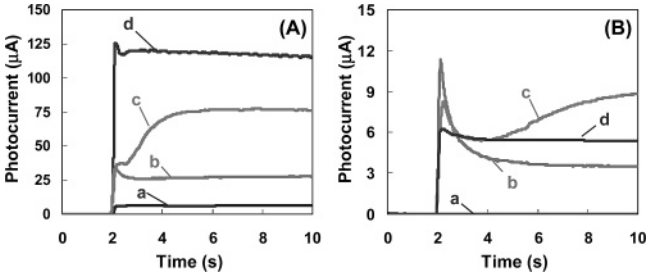

Figure 4. Photocurrent response of TiO_2 electrodes ((a) OTE/P-25, (b) OTE/(673 K-Ar)−TiO_2, (c) OTE/(873 K-Ar)−TiO_2, and (d) OTE/(873 K-Ar + O_2)−TiO_2)) to (A) UV ($\lambda > 300$ nm, intensity 13 mW) and (B) visible light ($\lambda > 420$ nm, intensity 23 mW) irradiation. The experimental conditions are the same as those in Figure 3.

OTE/(873 K-Ar + O_2)−TiO_2, exhibited the maximum photocurrent under UV light irradiation ($\lambda > 300$ nm). As compared to UV excitation, the photocurrent values obtained under visible light were smaller by about 1 order of magnitude. Since the absorption efficiency of the sputtered TiO_2 films is smaller in the visible than in the UV, we expected a smaller amount of incident photons to be harvested for light energy conversion. Despite the lower photocurrent generation efficiency, however, the results presented in Figures 3 and 4B confirmed the ability of the sputtered TiO_2 films to harvest visible photons for photocurrent generation.

It is interesting to note that the evolution of the photocurrent for the individual electrodes was also observed to be different. The donor density of these thin films has been investigated, and it was found that it was much higher for the film sputtered in Ar than in Ar + O_2. The donor density of these thin films changed in the following order: OTE/(873 K-Ar + O_2)−TiO_2 < OTE/(873 K-Ar)−TiO_2 < OTE/(673 K-Ar)−TiO_2. It is considered to be related to the surface states and affects the photocurrents of the individual electrodes since the surface morphology changed depending on the sputtering conditions, as shown in Figure 2 and Figure S1. The presence of different surface states lying within the band gap of TiO_2 has a significant impact in attaining photostationary conditions that involve charge separation, charge recombination, and charge transport following photoexcitation. The difference in the photocurrent time profiles was indicative of the fact that the sputtering conditions directly controlled the nature of the surface states. The TiO_2 film sputtered at higher temperatures (e.g., OTE/(873 K-Ar + O_2)−TiO_2) showed a steady photocurrent as compared to the film sputtered at lower temperatures. The initial decrease in the photocurrent of OTE/(673 K-Ar)−TiO_2 may arise from either the increase in the recombination rate with the increased trapping of the charge carriers during illumination or the mass transfer limitation of the hydroxide ions in the hole scavenging process. However, because of the high concentration of OH^- in the electrolyte (0.05 M), the second possibility is unlikely. When we decreased the concentration of NaOH by a factor of 10, the same pattern of photocurrent decay was observed. Furthermore, the films sputtered at higher temperatures did not exhibit a quick decay in the photocurrent. These results suggest that charge recombination at the surface state is an important factor in attaining a steady photocurrent flow for the sputtered TiO_2 thin films.

We have further investigated the photoinduced electric power characteristics of TiO_2 thin film electrodes by introducing a known resistance in the circuit. The current voltage response of the thin film electrodes under UV light irradiation are shown in Figure 5.

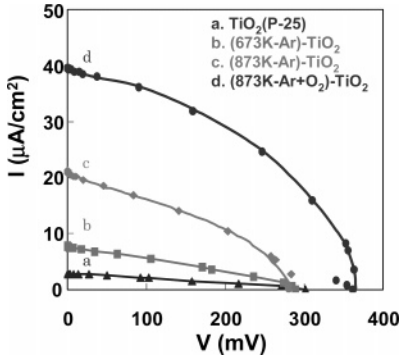

Figure 5. Current voltage characteristics of the photoelectrochemical cell employing different TiO_2 electrodes under UV light irradiation ($\lambda > 300$ nm).

TABLE 1: Photoelectrochemical Parameters of Various TiO_2 Thin Films at Relatively Low Excitation Intensity[a]

	excitation					
	$\lambda > 300$ nm (1.8 mW/cm^2)			$\lambda = 440 \pm 30$ nm (1.9 mW/cm^2)		
photoanode	I_{sc} (μA/cm^2)	V_{oc} (mV)	η (%)	I_{sc} (μA/cm^2)	V_{oc} (mV)	η (%)
P-25−TiO_2	2.8	301	0.01	0	0	
(673 K-Ar)−TiO_2	8.0	290	0.03	1.2	104	0.002
(873 K-Ar)−TiO_2	21.3	281	0.11	4.6	155	0.009
(873 K-Ar + O_2)−TiO_2	40.0	362	0.33	3.2	195	0.015

[a] Electrolyte: N_2-purged 0.05 M NaOH in water. Irradiation area: 0.5 cm^2.

TABLE 2: Photoelectrochemical Parameters of Various TiO_2 Thin Films at Relatively High Excitation Intensity[a]

	excitation			
	$\lambda > 300$ nm (13 mW/cm^2)		$\lambda = 440 \pm 30$ nm (23 mW/cm^2)	
photoanode	I_{sc} (μA/cm^2)	V_{oc} (mV)	I_{sc} (μA/cm^2)	V_{oc} (mV)
P-25−TiO_2	12.6	700	0.016	10
(673 K-Ar)−TiO_2	55.6	650	7	395
(873 K-Ar)−TiO_2	142	620	17	415
(873 K-Ar + O_2)−TiO_2	230	710	10.6	500

[a] Electrolyte: N_2-purged 0.05 M NaOH in water. Irradiation area: 0.5 cm^2.

As the applied load resistance decreased, an increase in the short circuit photocurrent and a decrease in the open circuit photovoltage (V_{oc}) could be seen. The cell parameters are summarized in Table 1. OTE/(873 K-Ar + O_2)−TiO_2 showed a remarkably large short circuit photocurrent of 40 μA/cm^2, an open circuit photovoltage of 362 mV, and a power conversion efficiency (η) of 0.33% at an incident light intensity of 1.8 mW/cm^2. A 440 nm band-pass filter, which allows the transmission of light in the wavelength range of 410−470 nm, was introduced in the excitation path to ascertain cell performance under visible light irradiation. All of the sputtered TiO_2 thin film electrodes showed visible light response, and OTE/(873 K-Ar + O_2)−TiO_2 exhibited a power conversion efficiency of 0.015%.

The performance of these electrodes at different light intensities was also evaluated. The open circuit voltage and photocurrents recorded at higher light intensity are summarized in Table 2. At higher incident intensities, the open circuit voltage and short circuit currents are higher as more of the incident photons are absorbed to create electron−hole pairs. However, the increased concentration of the charge carriers also resulted in an increased rate of charge recombination.

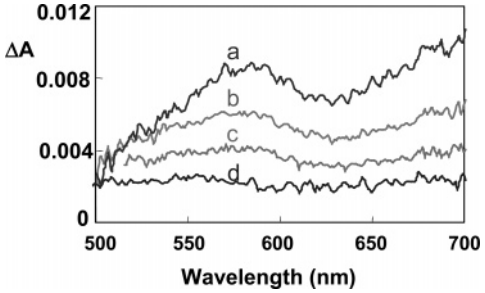

Figure 6. Transient absorption spectra recorded at (a) 0, (b) 100, (c) 250, and (d) 1000 ps after a 387 nm laser pulse excitation of the (673 K-Ar)−TiO_2 film.

Lifetime of Excited Electrons in the TiO_2 Particles. Transient absorption spectroscopy has been widely employed to probe the charge separation and charge recombination efficiency of semiconductor nanostructures following the band gap excitation of TiO_2 particles.[13,25−27] We employed femtosecond transient absorption spectroscopy to compare the behavior of photogenerated charge carriers in the sputtered films. The TiO_2 thin films were excited with a 387 nm laser pulse (pulse width 130 fs) and probed with a white light at different delay times. The transient absorption spectra recorded at different delay times for one of the samples are shown in Figure 6. The broad absorption of around 500−700 nm in the visible region represents the trapped electrons at the Ti^{4+} centers.[13,25−27] The appearance of this absorption in all three cases was prompt and completed within the laser pulse duration.

The absorption−time profiles recorded at 600 nm with short and long times after a 387 nm laser pulse excitation of the films are shown in Figure 7. The decay of the absorption recorded at 600 nm shows more complex kinetics and extends over a nanosecond time scale. The decay represents the lifetime of photogenerated electrons in the film and, hence, serves as a measure to compare the extent of charge separation for the different semiconductor nanostructures. Biexponential decay kinetics has been shown to accurately describe electron−hole recombination of surface-trapped electrons in quantum-sized TiO_2 solutions.[28] Since the decay shown in Figure 7 has been analyzed to fit the biexponential kinetics, it can be assigned mainly to electron−hole recombinations. Furthermore, earlier studies[26] have shown that the long-lived transient is assigned to interstitially trapped electrons in the interior of the nanocluster. Whereas the initial decay arises from the recombination of the surface-trapped electrons with the holes, the longer component of the decay involves the recombination of the interstitially trapped electrons with the holes.

The lifetimes obtained from analysis of the biexponential decay kinetics are summarized in Table 3. A comparison of the lifetimes of the three samples indicated that the electrons in OTE/(873 K-Ar + O_2)−TiO_2 survive for longer periods. Such a long survival of the photogenerated electrons in the TiO_2 films is essential in collecting them for photocurrent generation while the photocurrent generation efficiency presented in Table 1 supports this assumption. It was found that TiO_2 deposition under pure Ar gas plays an important role for the absorption of visible light and the presence of O_2 was important in minimizing charge recombination. The balance of Ar and O_2 during the sputtering procedure is especially important in the preparation of good photovoltaic cells.

In conclusion, visible-light-responsive TiO_2 thin films were successfully developed by an RF-MS deposition method in

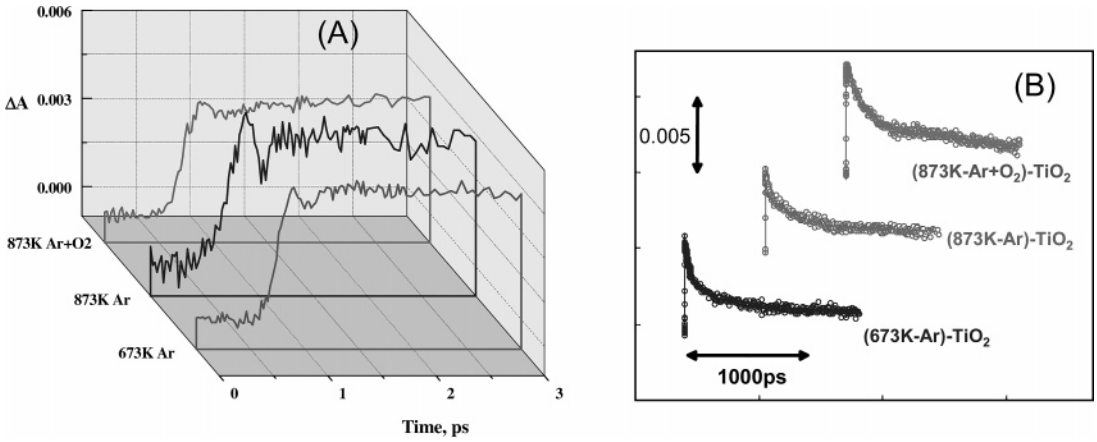

Figure 7. Absorption−time profile recorded at 600 nm following a 387 nm laser pulse excitation of the TiO_2 films The absorbance is plotted as a function of delay time of (A) 0−3 ps and (B) 0−1400 ps.

TABLE 3: Kinetic Parameters of the Charge Recombination Process for Various TiO_2 Thin Films

photocatalyst	a_1	τ_1 (ps)	a_2	τ_2 (ps)
(673 K-Ar)−TiO_2	0.305	54.7	0.177	723
(873 K-Ar)−TiO_2	0.171	72.2	0.201	502
(873 K-Ar + O_2)−TiO_2	0.375	105.6	0.241	905

which the substrate temperatures and the gaseous medium during deposition were controlled. The sputtered films showed higher IPCE values and power conversion efficiency in the UV light region than the commercial TiO_2 sample and exhibited a photocurrent response in the visible light region. OTE/(873 K-Ar)−TiO_2 showed the highest IPCE in the visible region (2.9% at $\lambda = 420$ nm) while OTE/(873 K-Ar + O_2)−TiO_2 exhibited the highest IPCE (12.6% at 350 nm) in the UV region with a power conversion efficiency of 0.33% at $\lambda > 300$ nm and 0.015% at $\lambda = 440 \pm 30$ nm. Femtosecond transient absorption spectroscopy experiments have revealed that the electrons in OTE/(873 K-Ar + O_2)−TiO_2 survive longer. It is evident that the films sputtered in the presence of Ar and O_2 at elevated temperatures provide the best combination of extending the absorbance into visible light regions and prolonging the lifetimes of the photogenerated electrons.

Acknowledgment. P.K. would like to acknowledge and express thanks to the Office of Basic Energy Science of the U. S. Department of Energy for their support. This is contribution No. NDRL 4644 from the Notre Dame Radiation Laboratory. This work was also supported by a "Grant-in-Aid for the Creation of Innovations through Business-Academic-Public Sector Cooperation" (No. 13308) from the Ministry of Education, Culture, Sports, Science and Technology of Japan. M.A. would like to express his thanks for their financial support.

Supporting Information Available: AFM images are illustrated in Figure S1. This material is available free of charge via the Internet at http://pubs.acs.org.

References and Notes

(1) Kamat, P. V. *Pure Appl. Chem.* **2002**, *74*, 1693.
(2) Anpo, M. *Res. Chem. Intermed.* **1989**, *11*, 67.
(3) Kamat, P. V. *Chem. Rev.* **1993**, *93*, 267.
(4) Anpo, M. *Pure Appl. Chem.* **2000**, *72*, 1265.
(5) Kalyanasundaram, K.; Graetzel, M. *Springer Ser. Chem. Phys.* **1984**, *39*.
(6) Anpo, M.; Takeuchi, M. *J. Catal.* **2003**, *216*, 505.
(7) Bard, A. J. *J. Photochem.* **1979**, *10*, 59.
(8) Kamat, P. V. Electron-Transfer Processes in Nanostructured Semiconductor Thin Films. In *Nanoparticles and Nanostructural Films*; Fendler, J. H., Ed.; Wiley-VCH: New York, 1998; p 207.
(9) Hoffmann, M. R.; Martin, S. T.; Choi, W.; Bahnemann, D. W. *Chem. Rev.* **1995**, *95*, 69.
(10) Serpone, N.; Pelizzetti, E. *Photocatalysis. Fundamentals and Applications*; John Wiley and Sons: New York, 1989.
(11) Crabtree, G. W.; Dresselhaus, M. S.; Buchanan, M. V. *Phys. Today* **2004**, *57*, 39.
(12) Dresselhaus, M. S.; Thomas, I. L. *Nature* **2001**, *414*, 332.
(13) Ikeda, S.; Sugiyama, N.; Pal, B.; Marci, G.; Palmisano, L.; Noguchi, H.; Uosaki, K.; Ohtani, B. *Phys. Chem. Chem. Phys.* **2001**, *3*, 267.
(14) Anpo, M.; Ichihashi, Y.; Takeuchi, M.; Yamashita, H. *Res. Chem. Intermed.* **1998**, *24*, 143. Anpo, M.; Ichihashi, Y.; Takeuchi, M.; Yamashita, H. *Stud. Surf. Sci. Catal.* **1999**, *121*, 305 (Proc. Tocat-3, Tokyo).
(15) Anpo, M. *Bull. Chem. Soc. Jpn.* **2004**, *77*, 1427.
(16) Irie, H.; Watanabe, Y.; Hashimoto, K. *Chem. Lett.* **2003**, *32*, 772.
(17) Diwald, O.; Thompson, T. L.; Zubkov, T.; Goralski, E. G.; Walck, S. D.; Yates, J. T. *J. Phys. Chem. B* **2004**, *108*, 6004.
(18) Umebayashi, T.; Yamaki, T.; Itoh, H.; Asai, K. *Appl. Phys. Lett.* **2002**, *81*, 454.
(19) Asahi, R.; Morikawa, T.; Ohwaki, T.; Aoki, K.; Taga, Y. *Science* **2001**, *293*, 269.
(20) Kitano, M.; Takeuchi, M.; Matsuoka, M.; Thomas, J. M.; Anpo, M. *Chem. Lett.* **2005**, *34*, 616.
(21) Matsuoka, M.; Kitano, M.; Takeuchi, M.; Anpo, M.; Thomas, J. M. *Top. Catal.* **2005**, *35*, 305.
(22) Torimoto, T.; Nakamura, N.; Ikeda, S.; Ohtani, B. *Phys. Chem. Chem. Phys.* **2002**, *4*, 5910.
(23) Vinodgopal, K.; Hotchandani, S.; Kamat, P. V. *J. Phys. Chem.* **1993**, *97*, 9040.
(24) Bedja, I.; Hotchandani, S.; Kamat, P. V. *J. Phys. Chem.* **1994**, *98*, 4133.
(25) Serpone, N.; Lawless, D.; Khairutdinov, R.; Pelizzetti, E. *J. Phys. Chem.* **1995**, *99*, 16655.
(26) Colombo, D. P. J.; Bowman, R. M. *J. Phys. Chem.* **1995**, *99*, 11752.
(27) Martini, I.; Hodak, J.; Hartland, G.; Kamat, P. V. *J. Chem. Phys.* **1997**, *107*, 8064.
(28) Colombo, D. P. J.; Roussel, K. A.; Saeh, J.; Skinner, D. E.; Cavaleri, J. J.; Bowman, R. M. *Chem. Phys. Lett.* **1995**, *232*, 207.